Journal of Alloys and Compounds 489 (2010) 638–644

Contents lists available at ScienceDirect

Journal of Alloys and Compounds

journal homepage: www.elsevier.com/locate/jallcom

High-temperature oxidation behavior of nanocrystalline diamond films

Jui-Chen Pu [a], Sea-Fue Wang [a,*], James C. Sung [b]

[a] Department of Materials and Mineral Resources Engineering, National Taipei University of Technology, 1, Sec. 3, Chung-Hsiao E. Road, Taipei, Taiwan
[b] KINIK Company, Taipei, Taiwan

ARTICLE INFO

Article history:
Received 8 October 2008
Received in revised form
22 September 2009
Accepted 23 September 2009
Available online 2 October 2009

Keywords:
High-temperature oxidation
Nanocrystalline diamond films
Thermal analysis
Raman analysis

ABSTRACT

In this study, high-temperature stability of nanocrystalline diamond films prepared by hot filament chemical vapor deposition (HFCVD) was investigated through differential thermal analysis/thermal gravimetric analysis (DTA/TGA), thermal analyses, visible and UV Raman analysis, and XPS analysis. Nanocrystalline diamond films with crystalline size of about 25 nm were obtained, which possess high density of grain boundaries with a high sp^2-bonding of non-diamond carbon. In the initial stage of oxidation, grain boundaries with non-diamond carbon and graphite phase were preferentially etched away by oxygen, which carries on with a faster rate. Then, a slower oxidation rate was continued through reacting the carbon atoms in rigid diamond structure with oxygen. The activation energies for former and the latter, calculated from the thermal analysis, are 195 and 217 kJ/mol, respectively. Both the results of in-situ Raman spectra and XPS spectra indicate that the carbon with sp^2-bonding significantly decreased with increasing temperature and soaking time.

1. Introduction

Diamond possesses excellent mechanical properties (hardness, strength, wear resistance), physical properties (high acoustic wave velocity, electron mobility, thermal conductivity, and optical transmission), and chemical properties (chemical and thermal stability, and radiation hardness) [1–3]. Diamond has many electronic and mechanical applications at high-temperatures, such as mold, cutting tool and heat sinks, and diamond stability is a critical parameter for engineering design. Among many film deposition routes, common diamond films were prepared via chemical vapor deposition (CVD). However, high surface roughness of these CVD diamond films places a major roadblock for various applications [4,5,6], such as SAW filters, laser window and field emission display [7–10]. This is the reason why efforts in CVD diamond films have diverted from conventional microcrystalline films to nanocrystalline films in the last few years.

Early studies have found that diamond grown under non-optimum conditions, such as lower hydrogen concentration or high methane concentration in the plasma [6,11], gives films with small grain size (e.g., several nanometers). Also, ions are not considered to be good for diamond growth since they enhance lattice disorder and also promote graphitic content in the deposit [11,12]. Nanocrystalline diamond films have large surface area and high density of grain boundaries which introduce abundant defects into the lattices [13,14]. Chen et al. and Balzaretti et al. used Raman spectroscopy to investigate the oxidation and graphitization of diamond films during heat treatment. They proposed that peak position, peak width, and intensity of Raman spectra changed with soaking time in air. The amount of non-diamond carbon phase reduces while the diamond grains remain stable as soaking time proceeded [15,16]. Taking advantage of its enhanced sensitivity, researchers [17,18] have shown that graphitization and oxidation of DLC result in decreasing the I_D/I_G ratio (intensity ratio of D and G bands of DLC), at high-temperatures. Studies of nanocrystalline diamond at high-temperature has increasingly drawn researchers' attention in recent years. Xu et al. used XRD to analyzed structure of the nanodiamond powder annealed in argon and found nanodiamond powder oxidation at 633 °C and graphitization at 751 °C. The cubic carbon structure decreases while the graphitic structure gradually increases with increasing annealing temperature [19,20]. Gogotsi et al. studied structural changes in nanodiamond after sintering at 1400 °C and 7 GPa. It indicates a strong increase in the relative intensity of the diamond peak and decrease of sp^2 carbon content in the nanodiamond sample, and increase in the average size of diamond grains [21]. Although substantial studies have been preformed on the critical factors that affect the thermal stability of diamond or DLC material, information on nanocrystalline diamond films is still critically lacking. It is therefore our motivation to investigate the variation of crystalline quality for nanocrystalline diamond films during annealing. Nanocrystalline diamond oxidation is important from application point of view. Oxidation of nanocrystalline diamond may be influenced by thermal treatment, reactive gases, and metal reaction at high-temperature. On

* Corresponding author. Tel.: +886 2 2771 2171x2735; fax: +886 2 2731 7185.
E-mail address: sfwang@ntut.edu.tw (S.-F. Wang).

0925-8388/$ – see front matter © 2009 Elsevier B.V. All rights reserved.
doi:10.1016/j.jallcom.2009.09.140

other hand, oxidation limits the temperature range and condition where nanocrystalline diamond can be effectively used. In this study, the diamond crystal, nanocrystalline diamond films, and graphite powder were prepared. The nanocrystalline diamond films were deposited on the (1 0 0) Si substrate using hot filament chemical vapor deposition (HFCVD) process. High-temperature stability properties, including morphology and structure of the nanocrystalline diamond films were investigated using differential thermal analysis/thermal gravimetric analysis (DTA/TGA), in-situ high-temperature Raman analysis with UV and visible lasers. Also, the results were interpreted through the effects of crystal size, crystal quality, structure and defects of the nanocrystalline diamond films. The relationship between the sp^3 and sp^2 bonds ratio and oxidation rate of nanocrystalline diamond films were discussed.

2. Experimental procedure

Nanocrystalline diamond films for this study were prepared using HFCVD method. Mixed source gases, hydrogen (H_2) with methane (CH_4), were fed into the chamber with a total reactor pressure of 20 Torr. Silicon wafer with (1 0 0) direction was used as substrate in this experiment. Ultrasonic pre-treatment by 0.5 μm diamond powder for 30 min was performed on the surfaces of silicon wafers to increase the nanocrystalline diamond nucleation [22]. Typical deposition conditions are as follows: filament temperature of 2000 °C, methane concentration of 5%, and the substrate temperatures at about 800 °C were used. The substrate temperature monitored by a Pt–Rh thermocouple was set just below the substrate. The deposition time read 60 h and the film thicknesses of nanocrystalline diamond films were 34 μm. More details about the preparation of diamond thin film can be found in our earlier reports [23].

Examinations were performed on the nanocrystalline diamond films. Crystallographic structure and crystallinity of the nanocrystalline diamond films were also characterized by X-ray diffraction (XRD, Rigaku D/max-B) using CuKα radiation. Surface morphological feature of the nanocrystalline diamond films were investigated by field emission scanning electron microscopy (SEM, HITACHI S-4700) and atomic force microscopy (AFM, Digital Instruments Nano Scope IIIA). Crystal quality and bonding structure of the nanocrystalline diamond films were further clarified by Raman spectroscopy (Jobin Yvon HR800UV). Visible and ultraviolet (UV) Raman spectra were excited using the 514 nm line of an Ar laser and 325 nm line of a He–Cd laser, respectively. Ratios of sp^3 and sp^2 bonds for the nanocrystalline diamond films were determined by the standard fitted on the five corresponding peaks (ν_1 and ν_3 mode, sp^3 peak, D and G bands) with Lorentzian-shaped band after subtracting background signal [24–28]. Binding energy and chemical composition of the nanocrystalline diamond films were characterized using high-resolution X-ray photoelectron spectrometer (XPS, PHI Quantera XPS Microscope) with a hemispherical analyzer.

DTA and TGA were subsequently performed on the nanocrystalline diamond films using a DTA/TGA system (PerkinElmer Pyris Diamond TG/DTA). Silicon substrate under the nanocrystalline diamond films was etched away using a 25 wt.% KOH solution at 80 °C before the DTA and TGA study. Samples, including single crystal diamond (De Beers, MBS-970), CVD nanocrystalline diamond films, and graphite powder (SHOWA, graphite, amorphous, −200 mesh, ((assay (as C) 80.0%, ignition residue 17.0%), were heated from room temperature to 1300 °C in air, at a heating rate of 50 °C/min. Oxidation kinetics were evaluated in the temperature range from 550 to 850 °C, using TGA analysis. Isothermal oxidization behaviors interpreted in term of weight-loss versus time for various samples were also characterized. The intensity change ratios of sp^3 and sp^2 bonds (ν_1 and ν_3 mode, sp^3 peak, D and G bands) of the samples were calculated, using a high-temperature visible and UV Raman analysis were compared at different temperatures in air for a soaking time up to 2 h, to provide the information of high-temperature oxidation.

3. Results and discussion

Fig. 1 shows the XRD patterns of the nanocrystalline diamond film, deposited using HFCVD method. The peaks at $2\theta = 43.9°$, 75.4° and 91.8° represent the diffractions from (1 1 1), (2 2 0) and (3 1 1) planes of diamond, respectively. It indicates that the (1 1 1) planes grow faster than other planes. Fig. 2 shows the surface SEM micrographs of nanocrystalline diamond film. Diamond phase with well-defined nano-scale crystalline facets was observed on the top surface. The predominantly surface morphology was ballast-like structures consisting of nanocrystalline size of about 25 nm, and high density of grain boundaries. The surface roughness of the surfaces of the nanocrystalline diamond films is about 72.7 nm according to the AFM results.

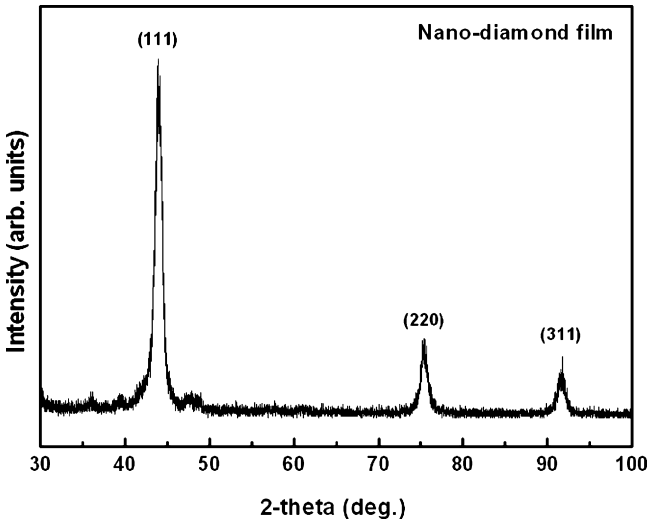

Fig. 1. XRD patterns of the nanocrystalline diamond film, deposited using HFCVD method.

Fig. 3 shows the Raman spectra of the nanocrystalline diamond film, measured by excitation energies of 514 nm (visible) and 325 nm (UV) laser. sp^2 bands contained in the nanocrystalline diamond films have a low band gap and are easily excited by visible light. So, the Raman scattering by 514 nm laser excitation from sp^2-bonded carbon should be ~100 times stronger than that from diamond regions. High sensitivity of visible Raman to the sp^2-bonded carbon phase was observed [28]. The visible Raman spectra of the nanocrystalline diamond film sample consist of bands near 1140, 1360, 1470, and 1550 cm^{-1} and a weak peak at 1335 cm^{-1}. A shoulder appears at approximately 1140 cm^{-1} in the spectra is due to the presence of nanocrystalline diamond [26,29]. Ferrari and Robertson proposed that two Raman features (1100–1200 and 1400–1500 cm^{-1}) are corresponding to trans-polyacetylene, or in other words, to sp^2-bonded carbon with the present of hydrogen [24]. They refer to the 1140 cm^{-1} peak as ν_1 mode, and to the 1470 cm^{-1} peak as ν_3 mode. These modes are roughly sum and difference combinations of C=C chain stretching and CH wagging modes [24–26,30,31].

The broad features of the visible Ramon spectrum at wavenumbers of 1360 and 1550 cm^{-1}, are the D and G bands, respectively. The D band referred to as the disorder structure of and non-diamond carbon phases, or nanocrystalline graphite. It is believed that the D band resulted from grain boundary defects. The G band

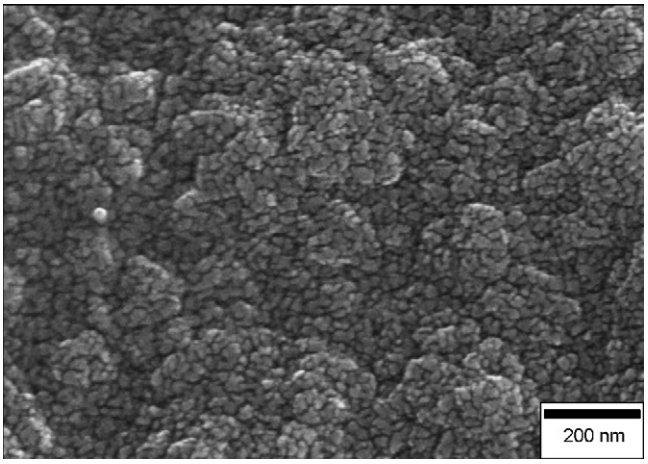

Fig. 2. SEM micrograph of the nanocrystalline diamond film.

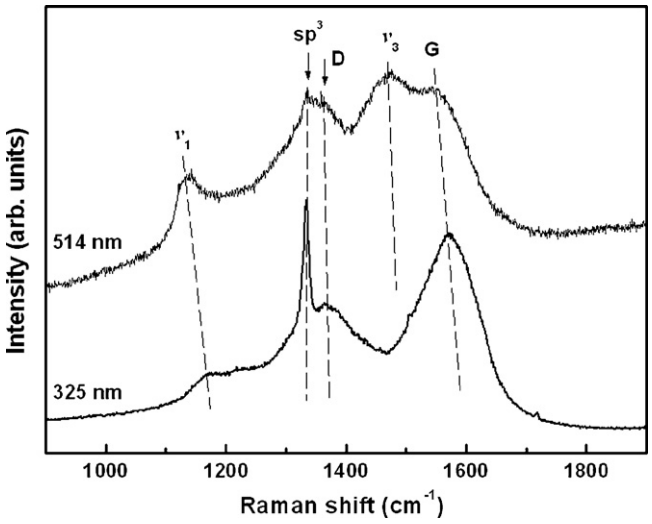

Fig. 3. Raman spectra for the nanocrystalline diamond film, measured by excitation energies of 514 and 325 nm lasers.

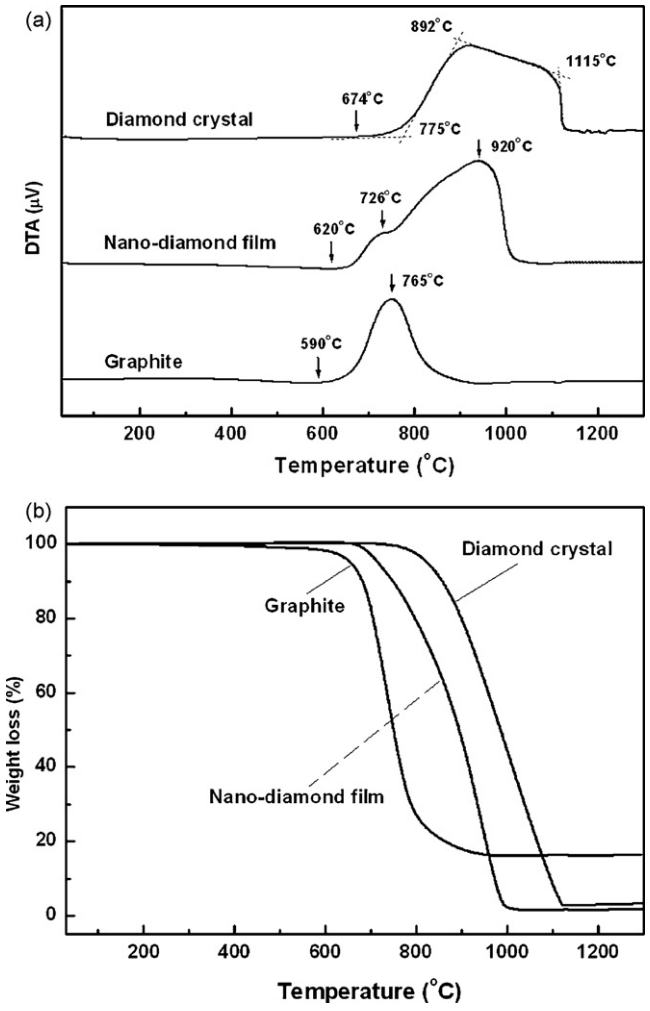

Fig. 4. (a) DTA and (b) TGA results of diamond crystal, nanocrystalline diamond film, and graphite measured in air.

(1550 cm^{-1}) is a relatively sensitive feature with respect to volume defects or graphite-like structures present in diamond films [6,27,29]. The weak broad peaks at 1335 cm^{-1} corresponds to diamond sp^3 bonds. The spectra in Fig. 3 indicate that the presence of the nanocrystalline size diamond with substantial amount of grain boundary and amorphous carbon (sp^2) in the films because it was prepared at high methane concentration [13,14].

In the UV Raman spectra from the 325 nm laser excitation, the peaks corresponding to sp^3 of diamond phase, non-diamond phases and graphite in the nanocrystalline diamond film are evident. Carefully comparing the Raman spectra from the 514 and 325 nm laser for the nanocrystalline diamond films, the intensities and the locations of the peaks for the sp^3 peak, D and G bands, v_1 and v_3 modes are different. The visible (514 nm) Raman spectra for the nanocrystalline diamond film have a weak sp^3 peak and an asymmetrically broadening of D and G bands, v_1 and v_3 mode. The peaks of v_1 mode, D band, v_3 mode, and G band at visible Raman spectra (1140, 1360, 1470, and 1550 cm^{-1}) for the nanocrystalline diamond film are shifted to lower wave numbers compared with those in UV Raman spectra (1170, 1362, 1530, and 1572 cm^{-1}). However, the sp^3 peak at 1335 cm^{-1} is not shifted in UV Raman spectra, due to the shorter C–C bond lengths and the higher vibrational frequencies [25,26]. The intensity of v_1 mode (≈1170 cm^{-1}) decreases and the v_3 mode (≈1530 cm^{-1}) disappears as the measurement performed using 325 nm laser excitation. This behavior is expected for sp^2-bonded configurations due to their smaller band gap. The intensity of sp^3 peak is higher in UV Raman spectrum than that in visible Raman spectrum because sp^3 sites have a wider band gap (5.5 eV) requiring a higher excitation energy [24–26].

Oxidation experiment of nanocrystalline diamond film was conducted at temperatures between room temperature and 1300 °C at a heating rate of 50 °C/min in air. Fig. 4(a) shows the DTA curves of diamond crystal, nanocrystalline diamond film, and graphite powders. It is evident that the oxidization of the diamond crystal begins at about 674 °C and finishes at about 1115 °C. The graphite powder begins at about 590 °C and maximizes at about 765 °C. The oxidation of predominantly graphite phase in nanocrystalline diamond film maximizes at about 726 °C, which is indicated by the knee in the DTA data. It is due to the oxidation of graphite and non-diamond phase preferentially located at surface and grain boundaries. Then the nanocrystalline diamond phase oxidizes at about 920 °C, which was lower than that of diamond crystal. This is because of more grain boundaries and defects and larger surface area-to-volume ratio in nanocrystalline diamond films [20].

Fig. 4(b) shows the corresponding TGA results of the nanocrystalline diamond films. The temperatures, at which rapid weight-losses occur due to oxidation, are coincident with the DTA results. The atomic oxygen reacts with nanocrystalline diamond film at the surface and forms CO and CO_2 products, that etches the carbon atom away from the surfaces [20,32]. Oxidation rate of the nanocrystalline diamond film lies between those of the graphite and diamond, because the contents of non-diamond carbons, defects and grain boundaries in nanocrystalline diamond film are more than those in diamond crystal. It thus leads to a lower oxidation temperature [13,14,26].

Fig. 5 shows the isothermal TGA curves of the diamond crystal, nanocrystalline diamond film, and graphite powder at 650 °C for soaking time up to 3 h. The results indicate that the weight-loss proceeded with soaking time, due to oxidation of the materials. Oxidation of the graphite powder at 650 °C is the fastest among the materials tested and then the nanocrystalline diamond film the second, and the diamond crystal the last. For the nanocrystalline diamond film, the slope of the weight-loss versus time curves, corresponding to the oxidation rate, changes with time. In the initial stage (first stage), the oxidation proceeds at a faster rate, which is probably due to the oxidation along non-diamond carbon and graphite phase. After the first stage, the rate of the weight-loss become small (second stage), which represents a different oxida-

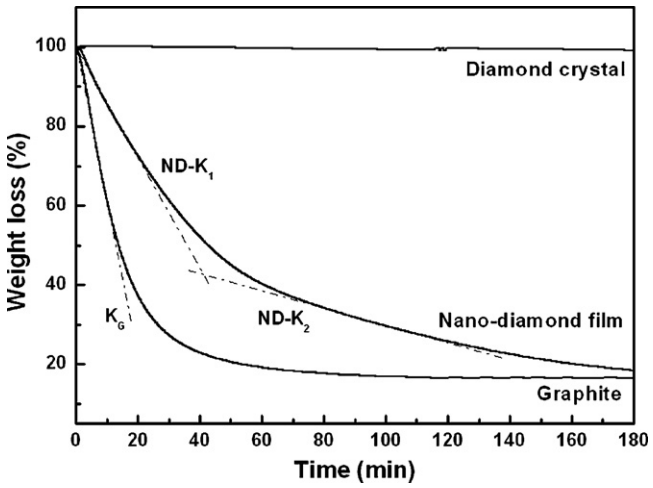

Fig. 5. Isothermal TGA results of diamond crystal, nanocrystalline diamond film, and graphite measured at 650 °C in air.

tion mechanism. It might be due to the oxygen reacts with carbon atoms in nanocrystalline diamond structure and etches through the rigid structures, which significantly lowers the oxidation rate. On the other hand, the diamond crystal sample does not have a detectable weight-loss and thus oxidation reaction when they were heated in air atmosphere up to 650 °C.

Fig. 6 shows the dependence of the oxidation rate on temperature in Arrhenius coordinates. The data points in Fig. 6 represent the oxidation rates, *K*, which is the slope of the weight-loss curve with respect to time, for the nanocrystalline diamond films and graphite powder from 550 to 850 °C. After curve-fitting, it was found that the activation energies, the slope of the line, for the nanocrystalline diamond films in the first stage and second stage were 195 and 217 kJ/mol, respectively. The activation energy of the first stage (195 kJ/mol) for the oxidation of nanocrystalline diamond films is close to that of graphite powder (173 kJ/mol), because the nanocrystalline diamond films contain non-diamond sp^2 phases. The oxidation activation energy for the second stage (217 kJ/mol) approximately coincides with that of the oxidation of CVD diamond films (211 kJ/mol). This is the same Johnson et al. reported data (213 kJ/mol) for CVD diamond films [32]. And other, the oxidation activation energy for the single crystal diamond is 258 kJ/mol. The two stages of oxidation with substantially different activation energies for nanocrystalline diamond films confirm the existence of two oxidation mechanisms [33,34].

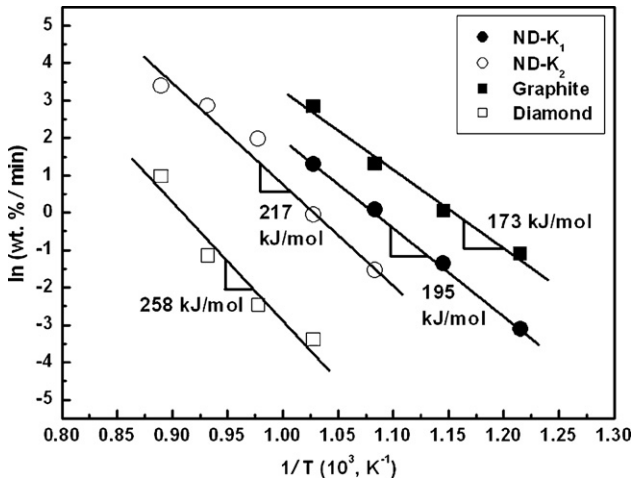

Fig. 6. Arrhenius plot of the isothermal oxidation for nanocrystalline diamond films and graphite in air.

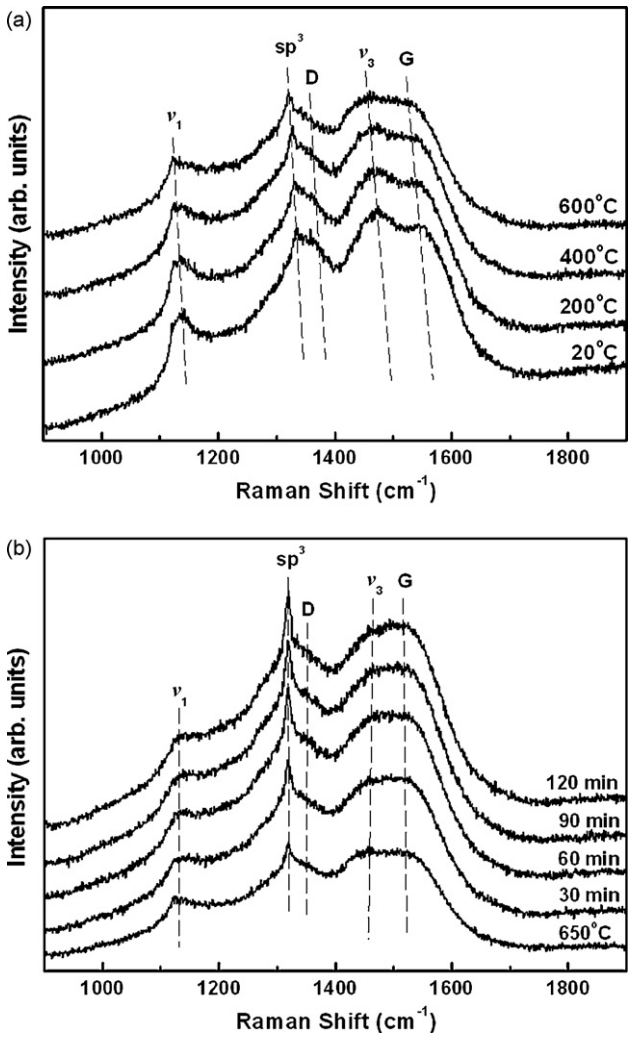

Fig. 7. (a) Visible (514 nm) Raman spectra for the nanocrystalline diamond film observed in air, (a) at different temperatures and (b) at 650 °C for various times.

Fig. 7(a) shows the variations of in-situ visible Raman spectra for the nanocrystalline diamond film observed at different temperatures in air. The five main features, v_1 and v_3 mode, sp^3 peak, D and G bands in Ramon spectra for the nanocrystalline diamond film, it indicates that the peak positions were shifted to a higher wave number and peak widths were broaden as the temperature increased. For instance, peaks located at 1140, 1335, 1360, 1470, and 1550 cm^{-1} at 20 °C were shifted to 1128, 1321, 1327, 1460, and 1543 cm^{-1} as the temperature increased to 600 °C. This is due to the thermal-expansion contribution, agreed well with those reported by Ferrari and Pfeiffer [24–26]. Fig. 7(b) shows the variations of in-situ visible Raman spectra for the nanocrystalline diamond films observed at 650 °C in air for various times up to 2 h. There was no noticeable shift of Raman peak position as soaking time increases. However, both Fig. 7(a) and (b) shows that the intensities of v_1 and v_3 mode decrease with increasing the temperature as well as the soaking time. Also, an increase in the relative intensity of sp^3 as a result of the selective oxidation of non-diamond phase and grain boundary defects [26,35,36].

Fig. 8(a) shows the variations of the UV Raman spectra for the nanocrystalline diamond film observed at different temperatures in air. It was known that UV Raman at 325 nm is directly sensitive to the sp^3 sites in diamond, which allows a direct probe

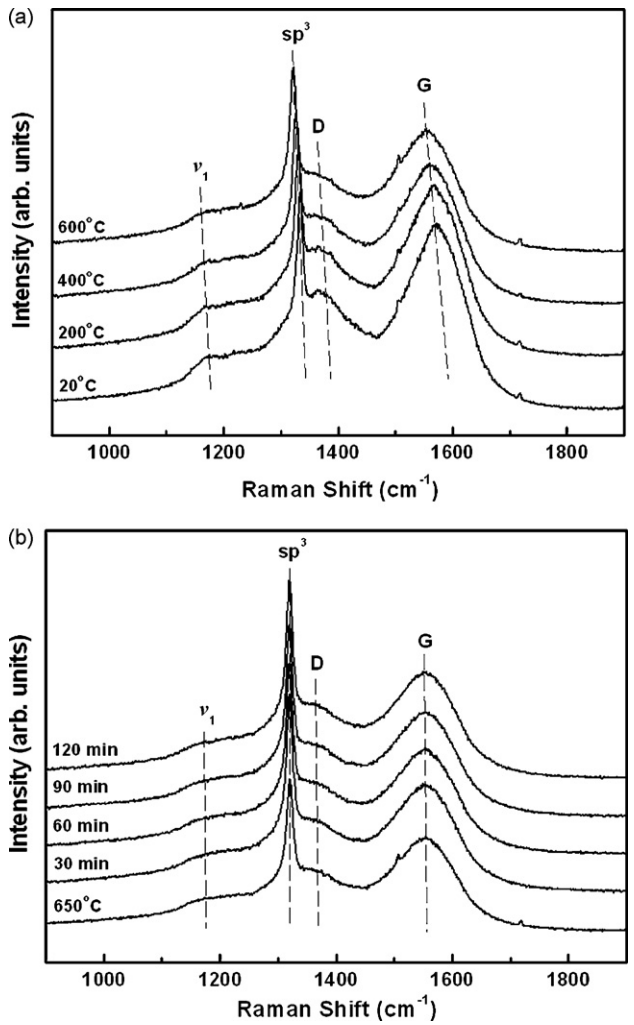

Fig. 8. (a) UV (325 nm) Raman spectra for the nanocrystalline diamond film observed in air, (a) at different temperatures and (b) at 650 °C for various times.

of sp^3 bonding. UV laser with high photon energy of 3.8 eV can excite both the π and σ states, and so is able to probe both the sp^2 and sp^3 sites. The spectra in Fig. 8(a) consist of four main features, v_1 mode, sp^3 peak, D and G bands. There is no sign of v_3 mode, because the v_3 mode (≈1530 cm^{-1}) is indistinct at 325 nm laser excitation [24–26]. The peaks corresponding to v_1 mode, sp^3 peak, D and G bands for the nanocrystalline diamond film are shifted to lower wave number and peak widths were broaden with increasing temperature. Fig. 8(b) shows the variations of in-situ UV Raman spectra for the nanocrystalline diamond films observed at 650 °C in air for various times up to 2 h. During isothermal 650 °C for 2 h, positions of Raman peaks were no found noticeable changes, but the relative intensity of the sp^3 band was increases and the sp^3 peak became sharpen as the soaking time increased. It was due to the oxidation of sp^2 bonded carbon which was easier than sp^3 bonded carbon.

Fig. 9 shows the variations of $I(sp^3)/I(sp^2)$ ratios for the nanocrystalline diamond films observed at isothermal 650 °C in air for soaking time up to 2 h. The $I(sp^3)/I(sp^2)$ ratios were calculated from UV Raman based on the sp^3 peak intensity versus the total intensity (sp^2) of v_1 mode, D and G bands. Increase in the $I(sp^3)/I(sp^2)$ ratios with soaking time for the nanocrystalline diamond film was observed when they were oxidized in air. The $I(sp^3)/I(sp^2)$ ratio increase with time, in which it begins at 0.6 and then saturated at a constant level of 0.74 after 20–40 min.

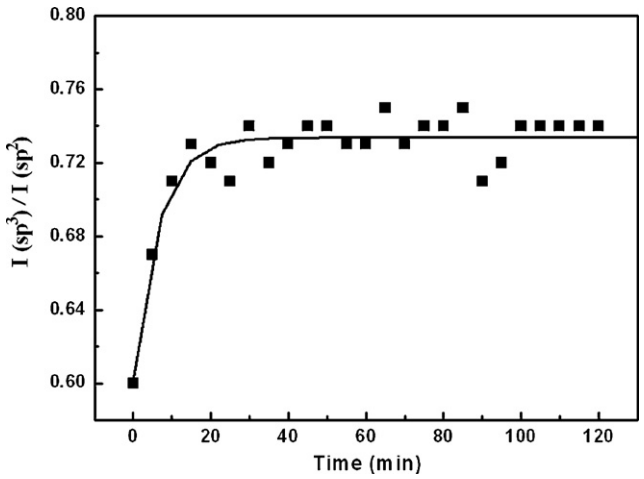

Fig. 9. The variation of $I(sp^3)/I(sp^2)$ ratios for the nanocrystalline diamond film calculated from UV (325 nm) Raman spectra of Fig. 8.

The increase in the $I(sp^3)/I(sp^2)$ ratio indicates that the oxidization on the surfaces of the nanocrystalline diamond film changes the crystal quality. However, It is more efficient for the oxygen to remove the graphite phase and non-diamond carbon from grain boundary at high-temperatures. Nanocrystallite diamonds embed-

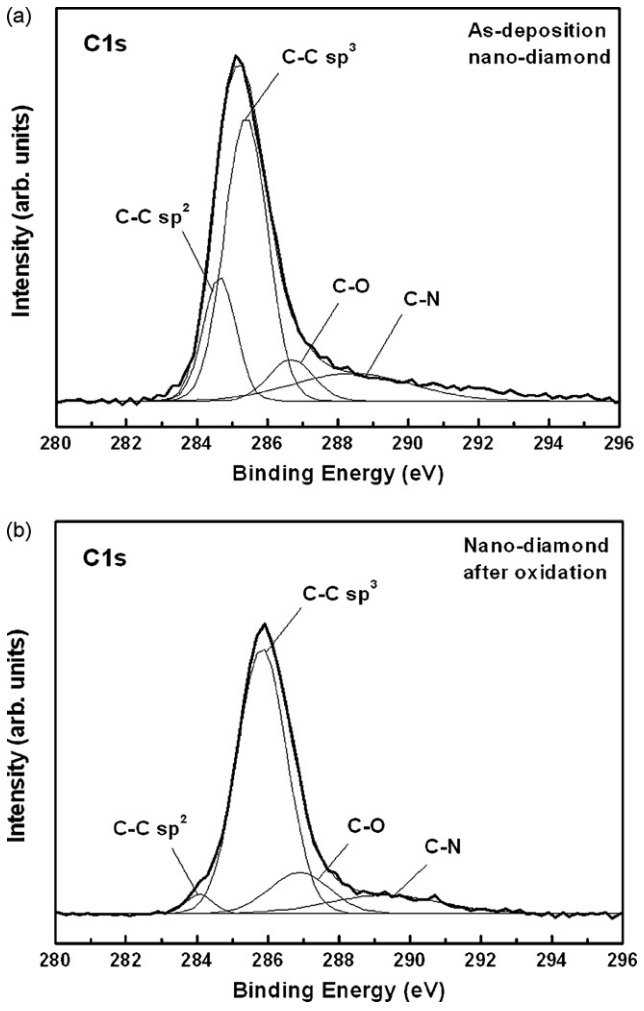

Fig. 10. XPS C 1s peak of the nanocrystalline diamond film: (a) as-deposited and (b) after oxidation in air at 650 °C for 1 h.

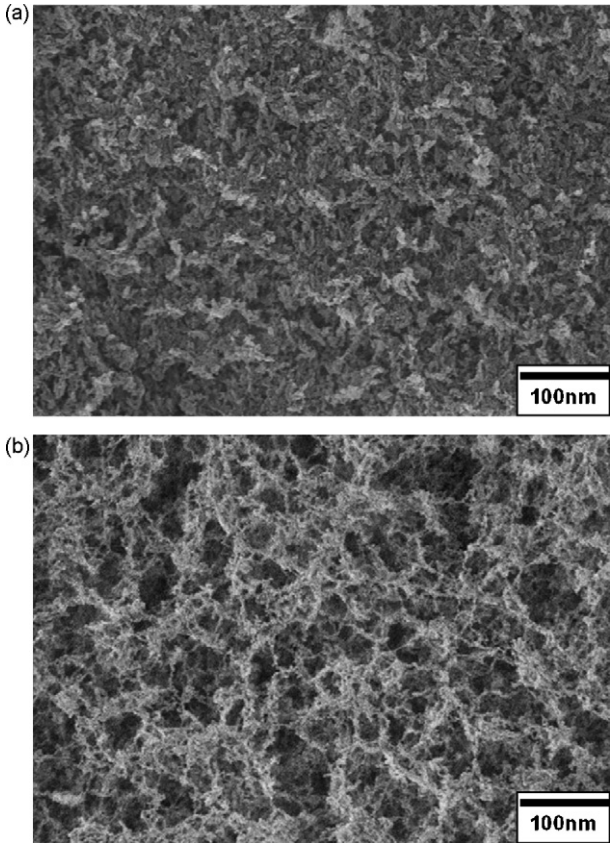

Fig. 11. SEM micrographs of the nanocrystalline diamond film, after oxidizing at 650 °C for (a) 10 min and (b) 30 min in air.

ded in a matrix of amorphous carbon [13,14], while oxidation for 2 h removes mainly amorphous carbon and other non-diamond species. This observation is consistent with that reported by Pfeiffer et al. [25,26,35,36].

Fig. 10(a) presents the XPS spectra of the as-deposited nanocrystalline diamond film. C 1s peak is located at 285.2 eV. The spectral line shape of the nanocrystalline diamond film suggests that it is composed of several components. The spectra were thus curve-fitted into four components with a Gaussian line shape. The binding energy of 284.4 eV is attributed as the sp^2 carbon bands and the binding energy of 285.8 eV is denoted as the sp^3 carbon bands. Peaks located at 286.3 and 289 eV are attributed to some C–O and C–N bonding formed at the surface of the nanocrystalline diamond film due to the absorption in air [37,38,39].

Fig. 10(b) shows the XPS spectra of the nanocrystalline diamond film after oxidation in air at 650 °C for 1 h. The C 1s photoemission spectra indicate an obvious structural change after oxidation reaction. The C 1s core level shifted 0.7 ± 0.1 eV toward high binding energy, which is correlated with a decrease in the sp^2 in the C 1s XPS spectra. A significantly decrease in the intensity of sp^2 peak in the nanocrystalline diamond film after oxidation was observed because the carbon atoms of sp^2 bands have been removed by oxygen atoms at high-temperature. The results are in good agreement with those obtained by Aleksenskiĭ et al. [37].

Fig. 11 shows the SEM micrographs of nanocrystalline diamond films, after isothermally oxidized at 650 °C in air for 10 and 30 min. A flake-like structure shown in Fig. 11(a) was obtained when the carbon atoms with weakly bonds at grain boundaries were preferentially etched away by oxygen during high-temperature oxidation [32]. Since nanocrystalline diamond grains are embedded in a-C matrix and grain boundaries are mostly decorated by sp^2-bonded carbon [13,14,26], which eventually leads to a sponge or branch structure as the oxidation process proceeds [Fig. 11(b)].

4. Summary

In this study, nanocrystalline diamond films were prepared by HFCVD. High-temperature stability of nanorystalline diamond films was investigated through DTA/TGA, thermal analyses, visible and UV Raman analysis, and XPS analysis. The results are summarized as follows:

1. The predominantly surface morphology of nanocrystalline diamond film was ballast-like structures consisting of nanocrystalline size of about 25 nm, and high density of grain boundaries. It possesses a higher sp^2 phase ratio of non-diamond carbon phase. During oxidation process, grain boundaries were preferentially etched away by oxygen at high-temperatures, which eventually leads to a sponge structure.
2. The initial stage of oxidation for nanocrystalline diamond film carries on with a faster rate which is probably due to the oxidation along non-diamond carbon and graphite phase. Then, the rate of the oxidation becomes small (second stage), which might be due to the oxygen reaction with carbon atoms in rigid diamond structure. The activation energies for former and the latter, calculated from the thermal analysis, are 195 and 217 kJ/mol, respectively.
3. In the in-situ Raman spectra of the nanocrystalline diamond film, the intensities of ν_1 and ν_3 mode, corresponding to trans-polyacetylene, decrease and the relative intensity of sp^3 bonds increases with increasing the temperature as well as the soaking time, as a result of the selective oxidation of non-diamond phase and grain boundary defects.
4. C 1s peak of XPS spectra were curve-fitted into four components with a Gaussian line shape. The binding energy of 284.4 and 285.8 eV are attributed to the sp^2 and sp^3 carbon bands, respectively. Peaks located at 286.3 and 289 eV are attributed to some C–O and C–N bonding formed at the surface of the nanocrystalline diamond film due to the absorption in air. The intensity of sp^2 peak in the nanocrystalline diamond film after oxidation was significantly decreased, due to the carbon atoms of sp^2 bands removed by oxygen atoms at high-temperature.

References

[1] J.E. Field, The Properties of Natural and Synthetic Diamond, Academic Press, London, 1992.
[2] J. Asmussen, D.K. Reinhard (Eds.), Diamond Films-Handbook, Marcel Dekker, New York, 2002.
[3] S.F. Wang, Y.F. Hsu, J.C. Pu, J.C. Sung, L.G. Hwa, Chem. Phys. 85 (2004) 432.
[4] D.G. Bhat, D.G. Johnson, A.P. Malshe, H. Naseem, W.D. Brown, L.W. Schaper, C.H. Shen, Diamond Relat. Mater. 4 (1995) 921–929.
[5] Y. Chen, L.C. Zhang, J.A. Arsecularatne, C. Montross, Int. J. Mach. Tools Manuf. 46 (2006) 580–587.
[6] H.S. Nalwa, Encyclopedia of Nanoscience and Nanotechnology, vol. 2, American Scientific Publishers, 2004, pp. 337–370.
[7] N. Jiang, K. Eguchi, S. Noguchi, T. Inaoka, Y. Shintani, J. Cryst. Growth 236 (2002) 577–582.
[8] M.D. Whitfield, B. Audic, C.M. Flannery, L.P. Kehoe, G.M. Crean, C. Johnston, P.R. Chalker, R.B. Jackman, Diamond Relat. Mater. 7 (1998) 533.
[9] K. Higaki, H. Nakahata, H. Kitabayashi, S. Fujii, IEEE 44 (6) (1997) 1395.
[10] T. Sharda, M.M. Rahaman, Y. Nukaya, T. Soga, T. Jimbo, M. Umeno, Diamond Relat. Mater. 10 (2001) 561–567.
[11] Y. Lifshitz, G.D. Lempert, E. Grossman, Phys. Rev. Lett. 72 (1994) 2753.
[12] W. Zhu, C.A. Randall, A.R. Badzian, R. Messier, J. Vac. Sci. Technol. A 7 (3) (1989) 2315.
[13] S. Bhattacharyya, O. Auciello, J. Birrell, J.A. Carlisle, L.A. Curtiss, A.N. Goyette, D.M. Gruen, A.R. Krauss, J. Schlueter, A. Sumant, P. Zapol, Appl. Phys. Lett. 79 (2001) 1441.
[14] X.T. Zhou, Q. Li, F.Y. Meng, I. Bello, C.S. Lee, S.T. Lee, Y. Lifshitz, Appl. Phys. Lett. 80 (2002) 3307.
[15] K.H. Chen, Y.L. Lai, L.C. Chen, J.Y. Wu, F.J. Kao, Thin Solid Films 270 (1995) 143.
[16] N.M. Balzaretti, J.A.H. da Jornada, Diamond Relat. Mater. 12 (2003) 290.

[17] R. Kalish, Y. Lifshitz, K. Nugent, S. Prawer, Appl. Phys. Lett. 74 (1999) 2936.
[18] R. Kalish, Y. Lifshitz, K. Nugent, S. Prawer, Surf. Coat. Technol. 120–121 (1999) 138.
[19] J. Chen, S.Z. Deng, J. Chen, Z.X. Yu, N.S. Xu, Appl. Phys. Lett. 74 (1999) 3651–3653.
[20] N.S. Xu, J. Chen, S.Z. Deng, Diamond Relat. Mater. 10 (2002) 249–256.
[21] G.N. Yushin, S. Osswald, V.I. Padalko, G.P. Bogatyreva, Y. Gogotsi, Diamond Relat. Mater. 14 (2005) 1721–1729.
[22] Y. Lifshitz, C.H. Lee, Y. Wu, W.J. Zhang, I. Bello, S.T. Lee, Appl. Phys. Lett. 88 (2006) 243114.
[23] S.F. Wang, Y.R. Wang, J.C. Pu, J.C. Sung, Thin Solid Films 498 (2006) 224.
[24] A.C. Ferrari, J. Robertson, Phys. Rev. B 63 (2001) 121405.
[25] R. Pfeiffer, H. Kuzmany, P. Knoll, S. Bokova, N. Salk, B. Gunther, Diamond Relat. Mater. 12 (2003) 268–271.
[26] H. Kuzmany, R. Pfeiffer, N. Salk, B. Gunther, Carbon 42 (2004) 911–917.
[27] A.M. Zaitsev, Optical Properties of Diamond: A Data Handbook, Springer, Germany, 2001, pp. 69–124.
[28] R.E. Shroder, R.J. Nemanich, J.T. Glass, Phys. Rev. B 41 (1990) 3738.
[29] T. Sharda, M. Umeno, T. Soga, T. Jimbo, Appl. Phys. Lett. 77 (2000) 4304.
[30] M. Yoshikawa, N. Nagai, M. Matsuki, H. Fukuda, H. Ishida, A. Ishitani, Phys. Rev. B 46 (1992) 7169.
[31] M. Yoshikawa, G. Katagiri, H. Ishida, A. Ishitani, T. Akamatsu, J. Appi. Phys. 64 (1988) 6464.
[32] C.E. Johnson, M.A.S. Hasting, W.A. Weimer, J. Mater. Res. 5 (1990) 2320.
[33] V.L. Kuznetsove, Yu V. Butenko, in: O.A. Shenderova, D.M. Gruen (Eds.), Ultrananocrystalline Diamond: Synthesis, Properties, and Applications, William Andrew Inc., NY, USA, 2006, p. 454.
[34] R.R. Nimmagadda, A. Joshi, W.L. Hsu, J. Mater. Res. 5 (1990) 2445.
[35] S. Osswald, M. Havel, V. Mochalin, G. Yushin, Y. Gogotsi, Diamond Relat. Mater. (2008).
[36] S. Osswald, G. Yushin, V. Mochalin, S.O. Kucheyev, Y. Gogotsi, J. Am. Chem. Soc. 128 (2006) 11635–11642.
[37] A.E. Aleksenskiĭ, Yu.V. Osipov, A.Ya. Vul, B. Ya Ber, A.B. Smirnov, V.G. Melekhin, G.J. Adriaenssens, K. Iakoubovskii, Phys. Solid State 43 (2001) 145–150.
[38] Yu.V. Butenko, S. Krishnamurthy, A.K. Chakraborty, V.L. Kuznetsov, V.R. Dhanak, M.R.C. Hunt, L. Šiller, Phys. Rev. B 71 (2005) 075420.
[39] Yu.V. Butenko, V.L. Kuznetsov, E.A. Paukshtis, A.I. Stadnichenko, I.N. Mazov, S.I. Moseenkov, A.I. Boronin, S.V. Kosheev, Fullerenes Nanotubes Carbon Nanostruct. 14 (2006) 557–564.